



# Enhancement of Mixing Performance of Non-Newtonian Fluids using Curving and Grooving of Microchannels

S. Baheri Islami<sup>†</sup> and M. Khezerloo

*Faculty of Mechanical Engineering, University of Tabriz, Tabriz, 51666-14766, Iran*

<sup>†</sup>Corresponding Author Email: [baheri@tabrizu.ac.ir](mailto:baheri@tabrizu.ac.ir)

(Received April 3, 2016; accepted September 29, 2016)

## ABSTRACT

In this study, a numerical investigation was performed on the mixing of non-Newtonian power-law fluids in curved micromixers with power-law indices between 0.49 and 1 and Reynolds numbers between 0.1-300. The properties of water and CMC solution were used for simulation of Newtonian and non-Newtonian fluid flows, respectively. The effects of grooves embedded on the bottom wall of micromixers and geometrical parameters such as depth and angle of grooves on mixing performance were examined. The mixing of non-Newtonian fluids using this kind of micromixers has not been studied before. Eventually, using of inclined grooves with 30° inclination angle was studied. Open source CFD code of OpenFOAM was utilized to simulate the mixing process. The results showed that the grooves caused chaotic advection and improved the mixing performance but had no significant effect on dimensionless pressure drop. Also, the grooves with 30° angle showed better mixing index for all values of power-law indices.

**Keywords:** Curved micromixer; Grooving; Chaotic advection; Non-Newtonian fluid; Mixing index.

## NOMENCLATURE

$C$	mass fraction	$U_m$	average velocity
$c_i$	mass fraction at sampling point $i$	$W$	channel width
$\bar{c}$	average mass fraction	$x, y, z$	cartesian coordinate axes
$D$	diffusion coefficient	$\dot{\gamma}$	shear rate tensor magnitude
$De$	Dean number	$\bar{\gamma}$	shear rate tensor
$D_h$	hydraulic diameter	$\delta$	geometry parameter
$H$	channel height	$\eta$	apparent viscosity
$H$	height of groove	$\theta$	angle of groove
$M$	mixing index	$\xi$	dimensionless geometrical parameter
$m$	consistency coefficient	$\rho$	density
$n$	power-law index	$\sigma$	standard deviation of mass fraction
$P$	pressure	$\tau$	stress tensor
$R$	microchannel radius of curvature		
$Re$	Reynolds number		
$U$	velocity vector		

## 1. INTRODUCTION

Micromixers are important components in microfluidic systems and have wide applications in bioengineering and chemical engineering fields. The mixing in low Reynolds number regime has many applications for example lab-on-a-chip (LOC) systems, chemical synthesis, polymerization, DNA analysis, biological screening enzyme assays, protein folding, drug delivery, detection/analysis of chemical or biochemical content.

Micromixers are classified into two categories: active and passive micromixers (Nguyen and Wu 2005). Active micromixers need external energy for mixing process, while mixing in passive micromixers is the consequence of the interaction between flow and channel geometry. The passive micromixers have special importance due to simple structure and easy fabrication. Chaotic micromixer is one of the passive micromixers. Utilization of the chaotic advection and secondary flows is a suitable method to increase the mixing efficiency in low

Reynolds numbers. The fluid flows become chaotic by creating the curvature in the channels. This curvature can be 3D or planar. Fabrication of the 3D serpentine micromixers requires multi-stage process whereas; the planar curved micromixers are fabricated in single-stage processes. Therefore, it is an advantage of planar curved micromixers.

There are several methods for fabrication of curved micromixers with grooves, for example photolithographic processes in silicon substrates. Also, alternative micromachining techniques such as laser-ablation, injection molding, hot-embossing, etc. are increasingly applied using polymer materials. On easy and cheap way to fabricate grooved micromixers is two-step photolithography process.

The clogging in microfluidic systems is an event that is usual, especially when working with polymeric solutions or cell suspensions. Also, clogging can be occurred because of reaction products. It can be avoided by establishing the flow configuration prior to introducing the reactants by using an inert stream. Suggested actions to unclog a micromixer include reversing the reaction, introducing a dissolving agent, and ultrasonic cleaning.

The grooved micromixers should be used carefully in the case of fluids mixing with big solid particles because of the grooves on the floor. However, the setup of these micromixers can be installed to allow for redundant operation mode. If a variation in pressure drop warns about the clogging, the system switches to another mixer and first mixer undergoes a cleaning cycle.

Numerous studies have been conducted on Newtonian fluids mixing in these types of micromixers. Vanka *et al.* (2004) studied the mixing in curved channel. This study was conducted for several Reynolds numbers between 0.1-20. They found that the mixing performance improved due to the secondary flows at high Reynolds numbers for curved channel, but mixing rate in straight channel reduced by increasing the Reynolds number. Scherr *et al.* (2012) studied a passive, planar micromixer design based on logarithmic spirals by experimental and numerical methods. They reported that the mixing efficiency declines by increasing Reynolds number until the minimum value of 53% at Reynolds number of 15 and then, the mixing efficiency increases to the maximum mixing efficiency of 86% at  $Re=67$ . Afzal and Kim (2013) presented a 3D numerical investigation of water and ethanol mixing in micromixers with sinusoidal walls. They examined the effect of the amplitude and pitch of sine wave on mixing index for Reynolds numbers between 0.1-30. They reported that in lower wave length, the dean vortices shifted toward the inner sinusoidal walls that it was an additional advantage of the sinusoidal structure over other serpentine micromixers. Also, they compared the mixing performance of sinusoidal micromixers with results of square wave and zig-zag wave micromixers and they observed that the sinusoidal micromixer showed better mixing performance than

other geometries. Tsai and Wu (2011) investigated several planar curved micromixers with radial baffles, both numerically and experimentally. They observed that the mixing efficiency improved due to the multidirectional vortices. In another study, Tsai and Wu examined three curved-straight-curved (CSC) micromixers, which had three inlets (Tsai and Wu 2012). They studied three different configurations for inlets and obtained the mixing efficiency and pressure loss between channel inlets and outlet for all cases and introduced the best configuration. The planar meandering micromixer with semi-elliptical side walls studied numerically and experimentally by Wu and Tsai (2013). They reported that the mixing was improved due to the multidirectional vortices include Dean and separation vortices. Mixing of water and ethanol in a new passive micromixer based on the concept of unbalanced splits and cross-collisions of fluid streams were studied numerically and experimentally by Ansari *et al.* (2010). The main channel was split into two sub-channels that subsequently recombine after a certain distance and the width of two sub-channels could be unequal. Their study was carried out for various ratios of sub-channel width and Reynolds numbers ranging from 10 to 80. They found that the Dean vortices appeared for all geometries at high Reynolds numbers and these vortices improved the mixing performance. But the micromixers with unequal sub-channels width achieved better mixing performance because the mixing is due to the combined effect of unbalanced collisions of the fluid streams and Dean Vortices. The groove embedded on the floor of the straight micromixers causes irregularities and increases the degree of mixing. These micromixers have similar application like other micromixers in biological and chemical industries but they have been used in specific applications such as effective and rapid mixing of sample and reagent, homogenization of solutions of reagents, analyte delivery to a biosensor surface, etc.

Du *et al.* (2010) evaluated effect of grooves on fluids mixing in straight micromixers. Their study was carried out numerically for two types of groove, slanted groove micromixers (SGM) and staggered herringbone micromixers (SHM). It was found that faster and finer mixing took place in the SHM. In order to increase the chaotic advection and find better mixing performance, using of grooves embedded on the floor of curved micromixers can be useful.

Alam and Kim (2012) investigated the fluids mixing in a curved micromixer with grooves in its side wall, numerically. They studied effects of geometric parameters on mixing performance and flow patterns in the range of Reynolds number 0.5 to 90. They reported that maximum enhancement of mixing index occurred for Reynold number 30 and it is 135% better than smooth microchannel. Both of the curved and smooth microchannels showed similar pressure drops. Also, they found that the width of grooves had a significant impact on the mixing index but the depth of grooves had

not more effect on mixing index. Cook *et al.* (2013) presented a novel micromixer used the benefits of secondary flows to improve the mixing performance. The micromixer included four curved segments that each of them contained nine inclined grooves on its bottom walls. They found good agreement between experimental and numerical results. The flow pattern and mixing performance in a micromixer with five curved grooved elements were studied numerically and experimentally by Cook and Hasan (2013). This study was performed for Reynolds numbers between 0.5-100. They stated that due to the change of dominant mixing mechanism, an increase-decrease trend for mixing index was observed by increasing the Reynolds number. Also, it was reported that the minimum and maximum mixing indices occur at Reynolds number 10 and 100, respectively. Many studies have been performed on mixing of non-Newtonian fluids in various kinds of micromixer. The mixing of non-Newtonian fluids in a helical static mixer was studied by Rahmani *et al.* (2004). They showed that the type of fluid had no significant effect on mixing performance at low Reynolds numbers, but this effect was important at high Reynolds numbers. A similar study for non-Newtonian power-law fluids in static mixer (SMX) was carried out by Liu *et al.* (2006). They evaluated the mixing performance by using the particle tracking technique. They reported that the shear-thinning fluids compared to Newtonian fluids, reached to higher mixing quality and lower pressure drop. Hadigol *et al.* (2011) studied the mixing of non-Newtonian fluids in 2D microchannel with nonuniform zeta potential distribution on walls. They found that the mixing efficiency decreased by increasing the Reynolds number. Also, the sensitivity of shear-thickening fluids to variation of Reynolds number was more than the one of shear-thinning fluids. A numerical study of mixing due to electrokinetically driven flow in a wavy serpentine microchannel for both shear-thinning and shear-thickening non-Newtonian fluids was performed by Cho *et al.* (2012). They used the power-law model to describe the non-Newtonian behavior of fluids. They studied the effects of various parameters such as power-law index, the wave amplitude, the wavy-wall section length, and the applied electric field strength on mixing performance. They found that for both types of fluid, the mixing performance increased by increasing the wave amplitude, extending the length of the wavy-wall section, and decreasing the strength of the electric field. Recently, Afzal and Kim (2014) studied the flow and mixing behavior of Newtonian and non-Newtonian fluid in T-shaped and serpentine microchannels. The properties of water and blood were selected for Newtonian and non-Newtonian fluid simulation, respectively. They reported that the serpentine channel achieved better mixing performance for all flow rates and the pressure drop for water was less than blood for similar flow rates.

Since the majority of fluids in engineering and biology applications are non-Newtonian, study on the mixing of non-Newtonian fluids in planar

curved micromixers is very important, whereas, considering the above mentioned entries, the effect of geometrical parameters of grooves as well as mixing of non-Newtonian fluids in grooved micromixers have not been studied yet.

In this study, mixing of Newtonian and non-Newtonian fluids in a Simple Curved (SC) micromixer was investigated. The effect of grooves embedded on its bottom wall and geometrical parameters of grooves such as depth and angle on mixing performance was examined. Eventually, the effect of grooves inclination on mixing performance was studied. As previously mentioned, micromixers are widely used for various applications in engineering and biological fields. The fluids flow in these processes cover wide range of Reynolds number. For example the velocity and Reynolds number in enzyme assay process are very small, whereas in some processes such as crystallization and polymerization are large (Jeong *et al.* 2010). This study was performed for shear thinning fluids ( $n=0.49-1$ ) at Reynolds numbers between 0.1-300. The molecular diffusion and the advection are the dominant mechanism at low and high Reynolds numbers, respectively. The range of Reynolds number was selected in a form that includes both mixing mechanism.

## 2. GEOMETRY AND GRID

Schematic diagram of the Curved micromixer with Groove (CG) and Curved micromixer with Inclined Groove (CIG) and their geometrical information are shown in Fig. 1. The height (H), width of the channel cross section (W) and axial length of all curved micromixers are 0.1 mm, 0.1mm, and 6mm, respectively. This study was carried out for two heights of the groove ( $h=15 \mu\text{m}$  and  $30 \mu\text{m}$ ) and three angles of groove ( $\theta=8.5^\circ$ ,  $6^\circ$  and  $3.5^\circ$ ). Also, the grooves of CG micromixer are in radial direction of the curved part of channel but grooves of CIG micromixer have an angle of  $30^\circ$  relative to this direction.

GAMBIT software was used to make hexahedral grids for all geometries. An example of the grid can be seen in Fig. 2.

## 3. GOVERNING EQUATIONS

The governing equations of three dimensional, steady and incompressible flows are continuity, momentum and species mass fraction convection-diffusion equation:

$$\nabla \cdot U = 0 \quad (1)$$

$$\rho U \cdot \nabla U = -\nabla P + \nabla \cdot \bar{\tau} \quad (2)$$

$$U \cdot \nabla C = D \nabla^2 C \quad (3)$$

where  $\rho$  is the fluid density, P is the pressure, C is the mass fraction, D is the diffusion coefficient and U is the velocity vector.

The shear stress tensor is given by:

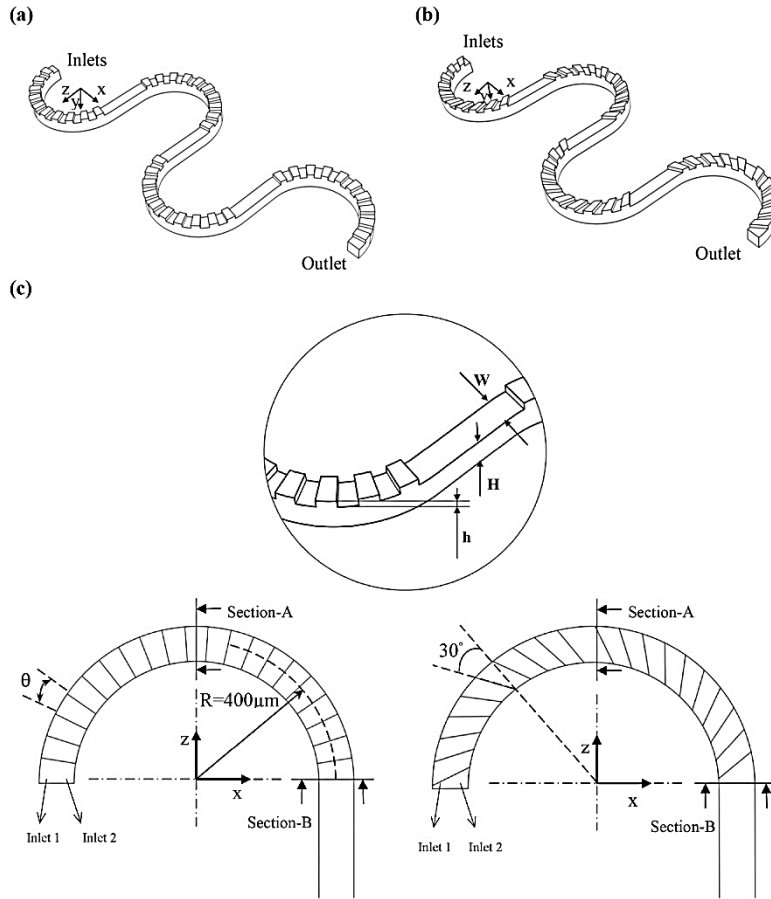


**Fig. 1. Schematic diagram of the (a) CG micromixer and (b) CIG micromixer, (c) geometrical information of CG and CIG micromixers.**

$$\overline{\tau} = \eta \overline{\dot{\gamma}} \quad (4)$$

where  $\overline{\dot{\gamma}}$  is the shear rate tensor, which is defined as

$$\overline{\dot{\gamma}} = \nabla U + \nabla U^T \quad (5)$$

$\eta$  is the apparent viscosity. For Newtonian fluids,  $\eta$  is constant and for non-Newtonian fluid it is dependent on shear rate tensor magnitude, which is written for power-law non-Newtonian fluids as:

$$\eta = m \dot{\gamma}^{n-1} \quad (6)$$

$$\dot{\gamma} = \sqrt{1/2(\overline{\dot{\gamma}} : \overline{\dot{\gamma}})} \quad (7)$$

where  $m$  and  $n$  are two parameters obtained by shear stress-shear rate curve fitting and called consistency coefficient and power-law index, respectively. For shear thinning fluids the apparent viscosity declines with shear rate so the power-law index has values between 0 and 1. The smaller the value of  $n$ , the greater is the degree of shear thinning.

The above equations were solved numerically using no-slip boundary condition at the walls, zero static pressure at channel outlet and fully developed velocity profile and zero-gradient pressure at both

inlets. Also, the mass fractions were set to be 1 at one inlet and 0 at another inlet.

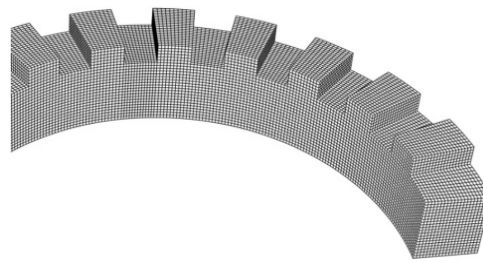


**Fig. 2. An example of hexahedral grid.**

Delplace and Leuliet (1995) presented an expression for the Reynolds number using the Metzner and Reed relation (1955). This equation is presented for power-law fluids flow in rectangular and square channels with different aspect ratios as:

$$Re = \rho U_m^{2-n} D_h^n / (m[(24n + \xi) / (24 + \xi)n]^n \xi^{n-1}) \quad (8)$$

This expression is based on a dimensionless geometrical parameter  $\xi$ . This parameter for square section channel with unity aspect ratio is equal to 7.113 (Delplace and Leuliet 1995). When fluid

flows through curved channel in addition to the viscosity and inertial forces another force affects the fluid motion, which is the centrifugal force. The interaction between inertial and centrifugal effects creates a radial pressure gradient that causes the generation of two counter-rotating vortices in transverse direction. The magnitude of inertial and centrifugal forces relative to the viscous forces one is expressed as a dimensionless number called the Dean number which is defined as:

$$De = \delta^{0.5} Re \quad (9)$$

where  $\delta$  is the geometry parameter, represents the centrifugal effects:

$$\delta = D_h / R \quad (10)$$

$R$  is the microchannel radius of curvature. In order to compare the efficiency of the micromixers, mixing index is defined as follows:

$$M = 1 - \sigma / \sigma_0 \quad (11)$$

Where  $\sigma$  is the standard deviation of mass fraction at a transverse cross section defined by the expression:

$$\sigma^2 = (1/k) \sum_{i=1}^k (c_i - \bar{c})^2 \quad (12)$$

with  $k$  denoting the total number of sampling,  $c_i$  is the mass fraction at  $i$ th cell, on the considered cross section, and  $\bar{c}$  is the average value of  $c_i$ .

$$\sigma_0^2 = \bar{c}(1-\bar{c}) \quad (13)$$

The mixing index will be between 1 and 0, where 0 represents the state before mixing, while  $M=1$  represents complete mixing.

### 3. NUMERICAL METHOD

The open source CFD code of OpenFOAM was used for performing the flow and mixing simulations. In this study, SIMPLE algorithm was used for pressure-velocity coupling. The second order upwind scheme and SFCD scheme (Self-filtered central differencing) (Ziman 1990) were selected for the discretization of convection terms in the momentum and species equations, respectively. The least square method was applied for the discretization of gradient terms. The iterations were continued until the relative residual for all variables becomes less than  $10^{-6}$ .

### 4. PROPERTIES OF FLUIDS

In this study water and CMC solution were used for simulation of Newtonian and non-Newtonian fluid flows, respectively. The density of water and CMC solutions (Srisamran and Devahastin, 2006) are  $1000 \text{ kgm}^{-3}$  and the consistency coefficient and power-law index of CMC solutions for various mass fractions are shown in Table 1. (Fellouah *et al.* 2010; Pinho and Whitelaw 1990). The power-law index is unit for water; consequently the

consistency coefficient is equal to the dynamic viscosity.

The diffusion coefficient was assumed  $3.6 \times 10^{-10} \text{ m}^2\text{s}^{-1}$  (Das and Chakraborty 2009). Also, by this assumption, the mixing effect caused by chaotic advection will be more evident.

**Table 1 Flow parameters of fluids (Fellouah *et al.* 2010; Pinho and Whitelaw 1990)**

CMC %	n (-)	m (Pa.s <sup>n</sup> )
0	1	0.000902
0.1	0.93	0.0066
0.2	0.85	0.0252
0.25	0.75	0.097
0.5	0.6	0.67
0.7	0.49	2.75

### 5. RESULTS

In order to validate the numerical results of Newtonian fluids, the mixing index for water flowing in CSC channel without baffles was simulated and compared with previous numerical results (Tsai and Wu 2011). It can be seen in Fig. 3. Also, the mixing of water in CSC micromixer with two baffles in each curved section, was simulated and mass fraction distributions on the horizontal mid-plane obtained and was compared with numerical and experimental results (Tsai and Wu 2011) (Fig. 4). Also, for the validation of non-Newtonian fluids mixing, the mixing index and velocity profile for impinging streams of shear-thinning fluid ( $n=0.6161$ ) was simulated and checked with results of Srisamran and Devahastin (2006) in Fig. 5. Considering Fig. 3, Fig. 4 and Fig. 5, the agreement between results is good.

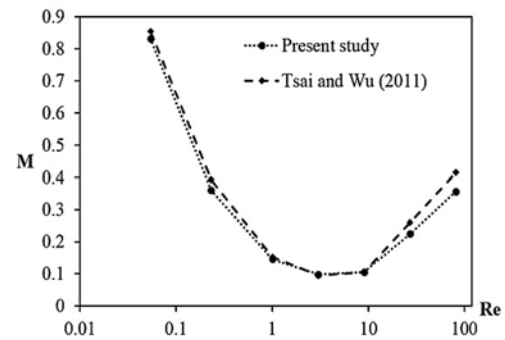


**Fig. 3. Comparison of mixing index for water flow in CSC channel without baffles.**

In another validation try, mixing of Newtonian fluids (water) in a micromixer based on fluid rotation was compared with experimental and numerical results of Cook *et al.* (2013). The fluid enters a meandering channel with four semicircular portions, each of which is lined with nine slanted grooves at the bottom surface and has been studied experimentally and numerically in this reference. The mixing index is presented in Table 2 and the results of present study and previous results (Cook

*et al.* 2013) have been compared. It can be seen that the agreement is acceptable.

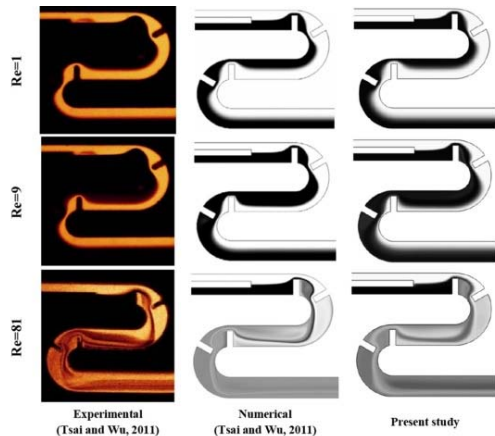


**Fig. 4. Comparison of the mass fraction distributions for water flow on the horizontal mid-plane of the CSC micromixer.**

**Table 2 Comparison present study with previous results (Cook *et al.* 2013)**

Re	1	5	10	25	50
Num. (Cook <i>et al.</i> 2013)	0.68	0.53	0.59	0.68	0.83
Exp. (Cook <i>et al.</i> 2013)	0.66	0.52	0.59	0.68	0.77
Present study	0.70	0.54	0.60	0.69	0.83
error % (relative to Num. results)	2.84	2.26	0.41	1.40	0.55
error % (relative to Exp. results)	5.50	4.20	1.80	1.27	7.46

There are many numerical studies on curved micromixers that were performed using uniform grids, (Tsai and Wu 2012, 2011; Cook *et al.* 2013; Cook and Hassan 2013) however in order to check the sensitivity of cell sizes near the wall both uniform and non-uniform grids were tested in this study for a shear-thinning fluid flow with  $n=0.75$  and  $Re=100$  in a SC-micromixer.

First, four different uniform grids were selected. The dimensionless velocity component in axial direction and mass fraction distribution, at line  $y=0$  on the section-A, for these grid sizes were obtained and is shown in Fig. 6(a) and (b). As it is evident, the grid with 380000 cells (with cell size of  $5 \mu m$ ) is sufficiently fine for the numerical calculation.

Then, two non-uniform grids were tested with  $1 \mu m$  and  $0.5 \mu m$  cell sizes near the wall. The dimensionless velocity component in axial direction and mass fraction distribution at line  $y=0$  on the

section-A are shown in Fig. 6(c) and (d). It is clear that the results are not sensitive to the cell size near the wall. It can be concluded that mesh independent results can be obtained using uniform grids, regardless of using fine grids near the wall.

As mentioned before, the apparent viscosity of non-Newtonian fluid depends on various parameters. These parameters are shear rate, power-law index and consistency coefficient. From Table 1, it can be realized that the consistency coefficient is different for various power-law indices. Fig. 7 shows the apparent viscosity on line  $y=0$  at the exit of the SC-micromixer for all fluids at  $Re=100$ . It is evident that the apparent viscosity increases by decreasing the power-law index increases.

Figure 8 shows the variation of mixing index with the Reynolds number in SC-micromixer for various values of power-law index. From Fig. 8 it can be seen that the degree of mixing has a decreasing-increasing trend. At first, the mixing index decreases by increasing Reynolds number because residence time of the fluid in the channel is reduced, and there is not enough time to molecular diffusion. After a minimum value the mixing index begins to increase. In this region, chaotic advection is the dominant mechanism of mixing. The chaotic advection and therefore mixing index increases with Reynolds number. Chaotic advection is created due to the centrifugal force that is applied to the fluid passing through curved part of mixer. The minimum value of mixing index occurs at a Reynolds number which called critical Reynolds number. It is the point where dominant mixing mechanism changes from molecular diffusion to chaotic advection. Also, the chaotic advection reduces due to the increasing of apparent viscosity, with decreasing the power-law index, and as a result the degree of mixing falls.

Figure 9 shows the mass fraction distribution and velocity vectors on Section-A of SC-micromixer ( $n=0.75$ ,  $De=0.5, 25, 100$ ). It is clear that the effect of centrifugal force becomes considerable by increasing Dean Number and both fluids move toward the external wall. The fluid in the core region is driven toward the outer wall by the centrifugal force. Fluid motion in the core region applies force to the fluid near the upper and lower walls to flow toward the inner wall and one-pair of counter-rotating vortices is generated. These are the so-called Ekman-vortices (Wanga and Cheng 1996). Intensity of Ekman vortices increases by increasing the Dean number and as a result the degree of mixing enhances.

Figure 10 shows the variation of mixing index versus the  $\theta$  for various Reynolds numbers and power-law indices. It can be seen that for all values of power-law index the groove angle has no considerable effect on mixing index at very low Reynolds number. But for flows with high Reynolds number, the mixing index increases by increasing the groove angle. Also, it is clear that the effect of Reynolds number becomes more considerable as power-law index increases.

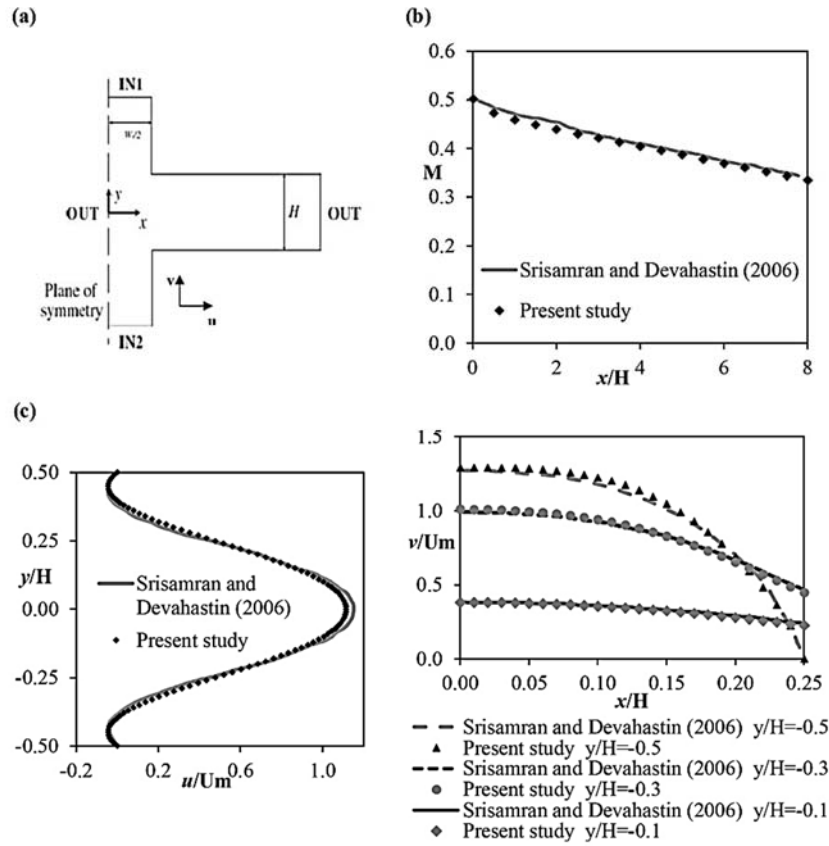


Fig. 5. Comparison of the results in a T-shape micromixer, (a) The studied geometry by Srisamran and Devahastin (2006), (b) Mixing degree along the channel, (c) The non-dimensional velocity in x and y direction.

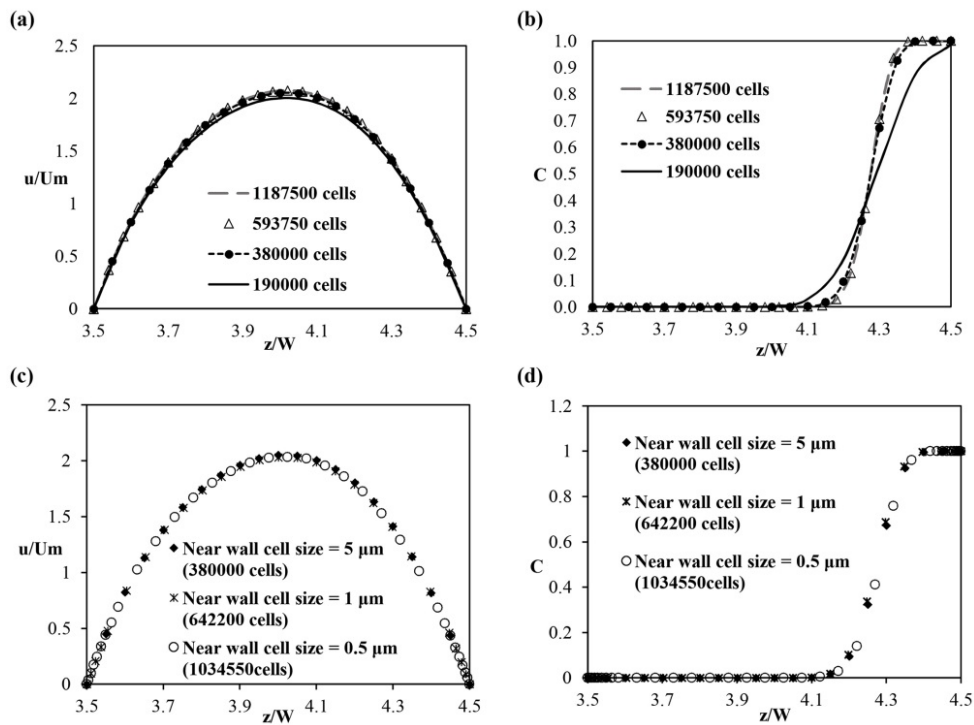
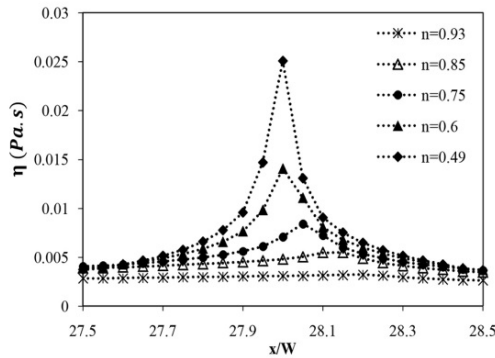
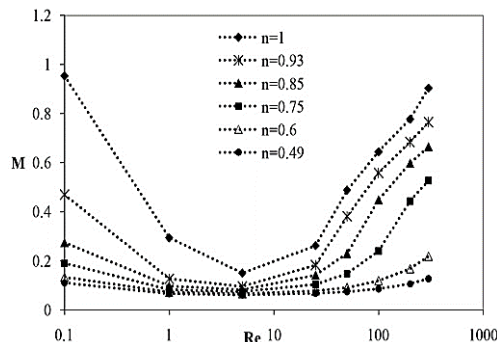


Fig. 6. Grid sensitivity tests,  $y=0$ , Section-A, SC-micromixer,  $Re=100$ ,  $n=0.75$ , (a) The non-dimensional velocity profile for various uniform grids, (b) Mass fraction distribution for various uniform grids, (c) The non-dimensional velocity profile for uniform and non-uniform grids, (d) Mass fraction distribution for uniform and non-uniform grids.

At high Reynolds numbers of non-Newtonian fluids flow, due to the high fluid velocity, the groove with small angle is not able to deflect the flow direction, so the mixing index does not improve, but higher angles can dominate the inertia forces of Reynolds numbers and lead to higher mixing degrees. However, for  $n=0.6$  and  $0.49$  the mixing enhances with small angle even at high Reynolds numbers. It is because of the higher effective viscosities in such power law indices that weaken the inertia forces and make flow deflection effects more considerable.



**Fig. 7. The apparent viscosity for all values of power-law indices at  $y=0$  at the exit of the SC-micromixer,  $Re=100$ .**



**Fig. 8. Variations of the mixing index with the Reynolds number at the exit of the SC-micromixer for various power-law indices.**

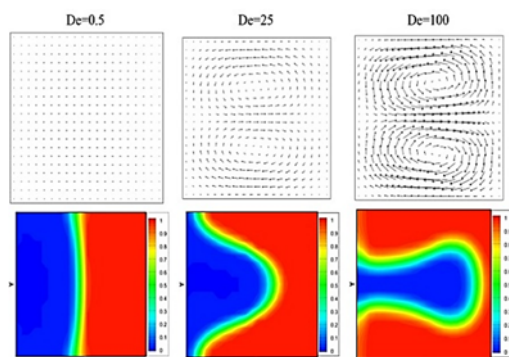


**Fig. 9. Mass fraction distribution and velocity vectors on Section-A, SC-micromixer,  $n=0.75$ .**

The variation of mixing index versus the groove depth for various Reynolds numbers and power-law

indices can be seen in Fig. 11. It can be seen that for all values of power-law indices the groove depth has no effect on mixing index at very low Reynolds numbers, while for high Reynolds numbers, the results show an increase in degree of mixing by increasing groove depth. As Reynolds number increases, thickness of boundary layer decreases and the flow can enter and exit the deeper grooves. It causes the strengthening of chaotic advection at high Reynolds numbers and therefore improving the mixing.

Figure 12 shows the mass fraction distribution on Section-B and center plane of three micromixers, SC, CG and CIG for  $n=1$  at  $Re=50$ . As Fig. 12(a) shows, two liquids enter the micromixer and flow in curved section. The chaotic advection is created due to centrifugal force which leads to the transversal flow and species rotation. Location (A) is the onset of species rotation at  $\beta=110^\circ$ . At  $\beta=135^\circ$ , that is being showed by location (B), the order of two fluids has been changed completely. Figure 12(b) shows that the mentioned angles are  $65^\circ$  and  $105^\circ$  and occur at locations (A') and (B'), respectively. These angles are less than those of SC micromixer. It is clear that embedding the groove on the bottom of the micromixer increases the irregularities, so the species rotation occurs at smaller angles. For CIG micromixer the first species rotation starts at location (A''),  $\beta=50^\circ$  and completes at (B''),  $\beta=70^\circ$  as shown in Fig. 12(c). These angles are less than those of SC and CG micromixers. Even, another species rotation can be seen at location (C''). In CIG micromixer, with inclined grooves on the walls, the grooves direct fluid from the outer wall toward the inner wall. So in addition to the centrifugal force, up-down movement of fluids between grooves improves the mixing performance.

Figure 13 shows the mass fraction distribution on section-B and mid plane of three micromixers, SC, CG and CIG for  $n=1$  and  $0.6$  at  $Re=0.1$ . As can be seen, radial grooves on the bottom wall of micromixer do not have significant effect on the distribution of mass fraction for both “n” values at very low Reynolds number, while they are effective at higher Reynolds numbers (Fig. 12). The mass fraction distribution on section-B shows that the flow rotation and species location change occur due to the directing of outer species toward the side of inner wall. For  $n=0.6$  significant rotation is not observed in SC and CG micromixers and mixing is due to the molecular diffusion. But locations (D) in CIG micromixer show the slight rotation. It increases the interface between two fluids as well as the molecular diffusion.

Figure 14 shows the variation of mixing index versus Reynolds number for all values of power-law index and three micromixers, SC, CG and CIG with  $h=30 \mu\text{m}$  and  $\theta=8.5^\circ$ . It can be seen that for all values of  $n$ , the SC and CG micromixers have nearly the same mixing index at very low Reynolds numbers ( $Re=0.1$  and  $1$ ), whereas the CG micromixer shows significant improvement in the mixing index at moderate and high Reynolds numbers ( $Re>1$ ). As shown in Fig. 14 for all cases, the maximum mixing index is related to CIG

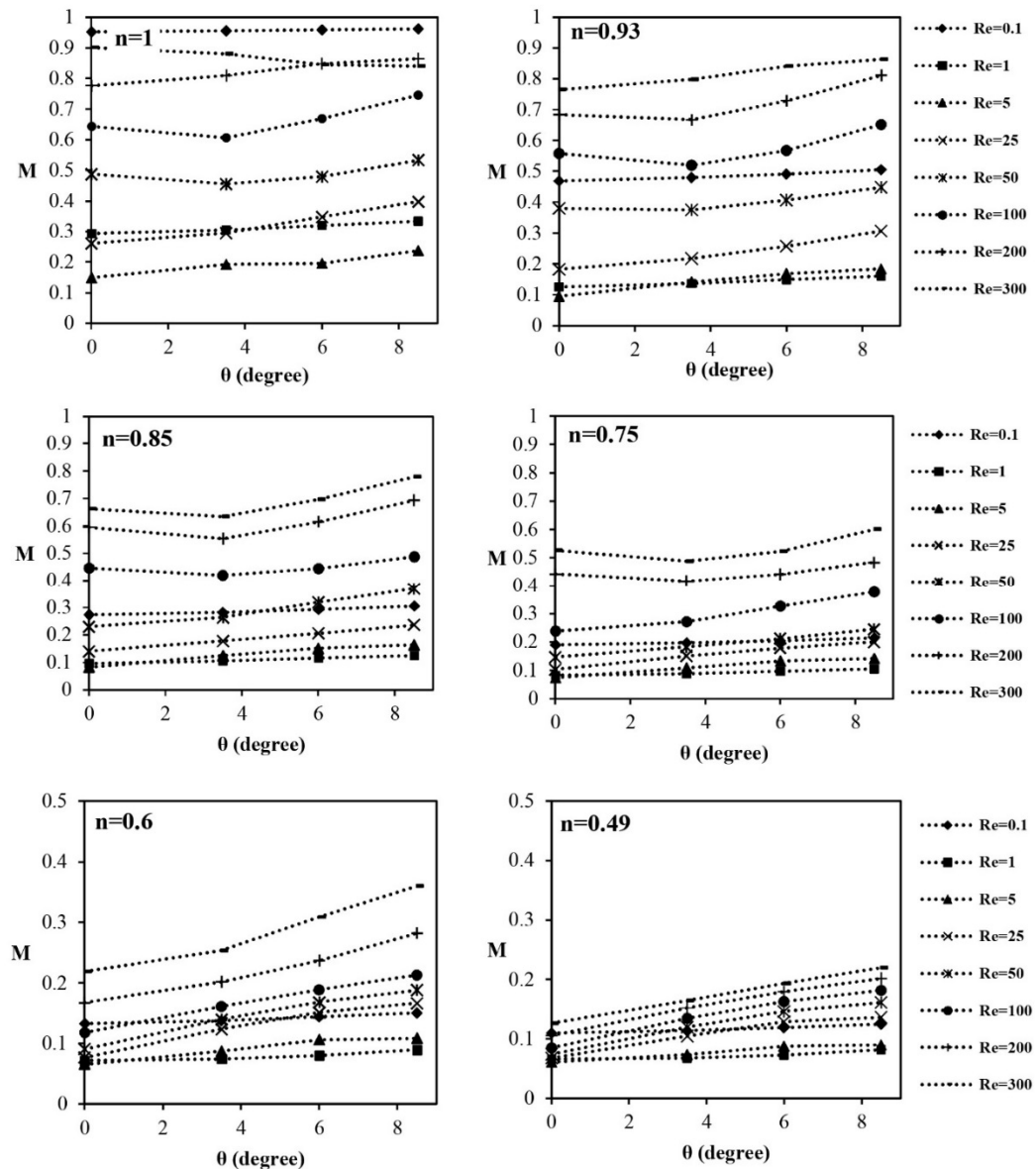


**Fig. 10.** Variation of mixing index versus the angle of groove for various power-law indices, CG micromixer,  $h=30 \mu\text{m}$ .

micromixer. It shows that the outer fluid is directed toward the inner wall by inclined grooves in CIG micromixer. It is the main reason of mixing enhancement at low Dean numbers. At higher Dean numbers, this effect is added to the effect of centrifugal force and causes the increasing of mixing index.

The pressure drop is an important factor, because it directly affects the required input energy of mixing process. In order to investigate the pressure drop in SC, CG and CIG micromixers, the dimensionless pressure drop was defined as  $\Delta P/\rho U_m^2$ . Figure 15 shows the variation of dimensionless pressure drop versus the Reynolds number for all values of power law index and three micromixers. The dimensionless pressure drop decreases rapidly by increasing the Reynolds number for all values of  $n$ . Also, as can be

seen, the dimensionless pressure drop for all values of power-law indices except for values which are close to unit (e. g.  $n=1$  and  $n=0.93$ ), depends on geometry of micromixers. Fluids with lower value of  $n$ , have strong shear thinning behavior. It means when larger shear stress is applied to fluid, apparent viscosity of fluid decreases. So, although GC and IGC micromixers applied larger shear stress to fluid in comparison with SC-micromixer, they all have same dimensionless pressure drop, because apparent viscosity decreases in these cases and counteracts the increase of dimensionless pressure drop caused by grooves, while for fluid with  $n=1$  or  $n=0.93$ , it can be seen that there to be grooves has an effect on dimensionless pressure drop and causes an increase. Since shear thinning behavior of these fluids is either very weak (e. g.  $n=0.93$ ) or does not exist at all (e. g.  $n=1$ ).

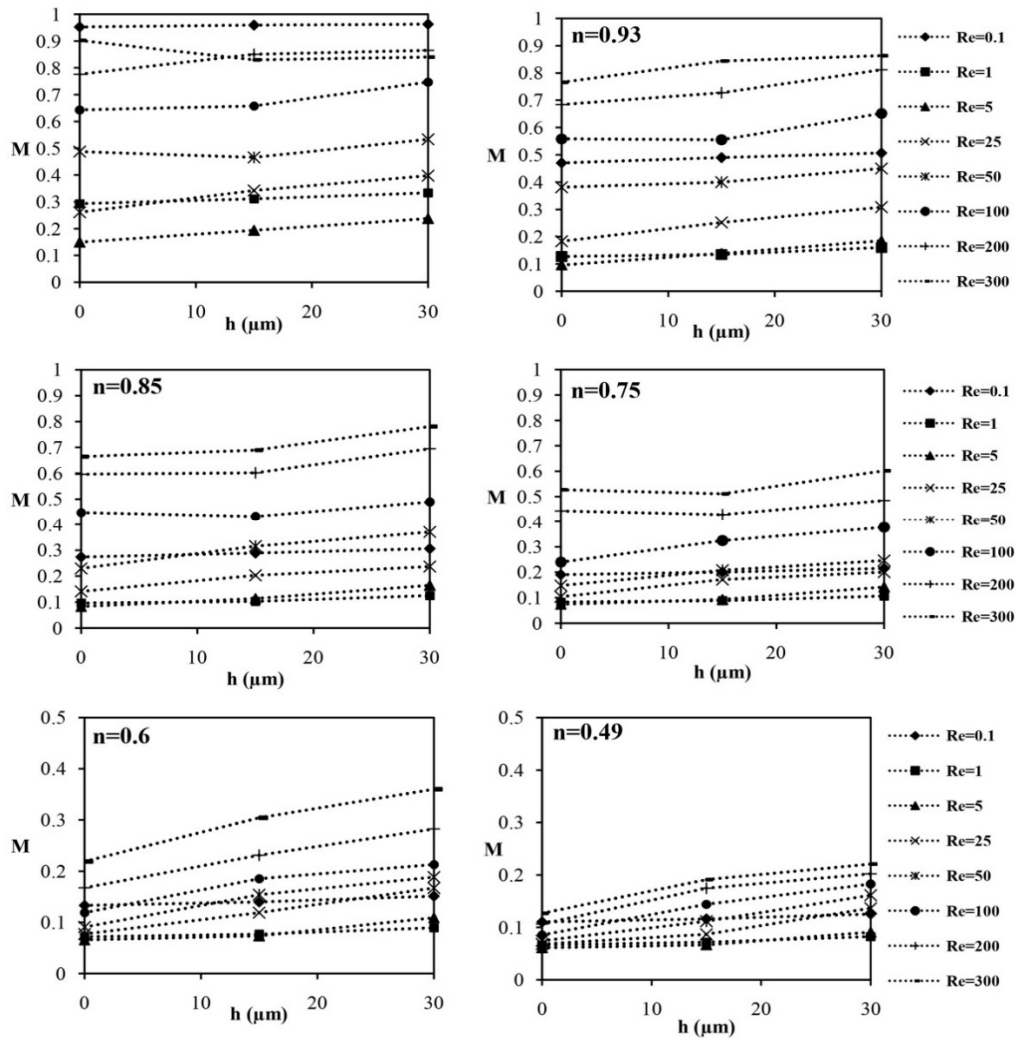


Fig. 11. Variation of mixing index versus depth of groove for various power-law indices, CG micromixer,  $\theta=8.5^\circ$ .

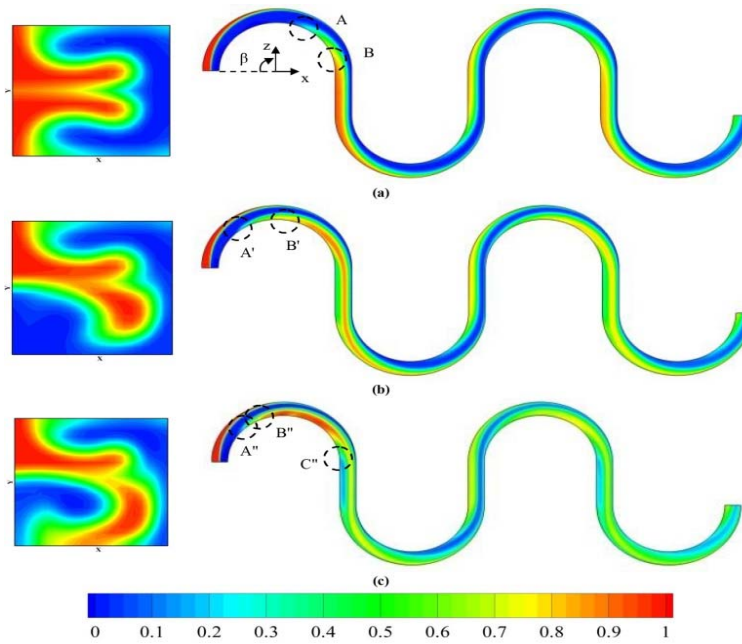
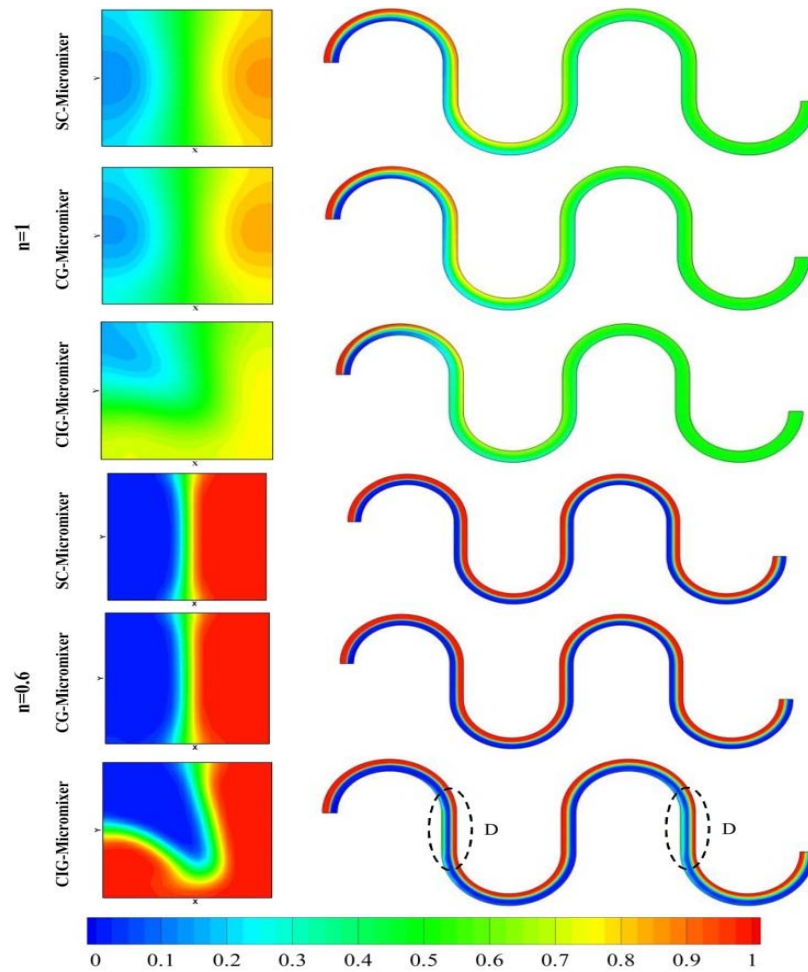


Fig. 12. Mass fraction distribution on Section-B (left) and center plane (right) of three micromixers, (a) SC-micromixer, (b) CG-micromixer and (c) CIG-micromixer,  $n=1$ ,  $Re=50$  ( $De=25$ ),  $h=30 \mu\text{m}$ ,  $\theta=8.5^\circ$ .



**Fig. 13. Mass fraction distribution on Section-B (left) and center plane (right) of three micromixers, SC, CG and CIG,  $n=1$  and  $0.6$ ,  $Re=0.1$  ( $De=0.05$ ),  $h=30 \mu\text{m}$ ,  $\theta=8.5^\circ$ .**

Also, it can be seen that the embedding of grooves in bottom wall of micromixers has no effect on dimensionless pressure drop.

Figure 16 shows the streamlines of CIG-micromixer on Section-B for  $n=0.85$  and three Reynolds (or Dean) numbers. It can be seen that the streamlines at  $Re=1$  ( $De=0.5$ ) deviate slightly from the horizontal lines and two counter rotating vortices form in the transverse plane by increasing the Reynolds (Dean) number and these vortices become bigger and stronger as the Reynolds (Dean) number increases. This is due to the centrifugal force strengthening and embedding the inclined grooves on the bottom of the micromixer, as mentioned before.

Figure 17 shows the streamlines of CIG-micromixer on Section-B for various power-law indices at  $Re=50$ . As previously mentioned, the apparent viscosity increases by reducing the power-law index, so the flow of shear thinning fluids is more affected by viscous force and the chaotic advection within the fluid flow is low. Also, the size and intensity of transversal vortices (Ekman vortices) increase with power-law index.

It is evident from Fig. 16 and Fig. 17 that the vortices are not symmetric relative to each other. It is because of the presence of grooves on the bottom wall that changes the flow patterns in comparison to the top wall.

In a steady flow, the particle trajectories comply with the streamlines and the velocity vectors are tangent to the streamlines at any point of the computational domain (Wang *et al.* 2003). The streamlines within the micromixers show more details about the bulk advection. The massless particles released from the vertical line in the middle of the inlet-2 and the streamlines along the two turns are shown in Fig. 18 for three types of micromixers. It is clear that the streamlines near the bottom wall in CIG-micromixer entered into the grooves and traveled toward the inner wall, so the streamlines become irregular even at low Reynolds number ( $Re=1$ ), while the streamlines in the other two micromixers are more regular. It can be stated as a result that at high Reynolds (Dean) numbers in addition to the centrifugal force, the inclined grooves cause the chaotic flow and therefore increase the mixing degree.

Different methods are used to enhance the mixing

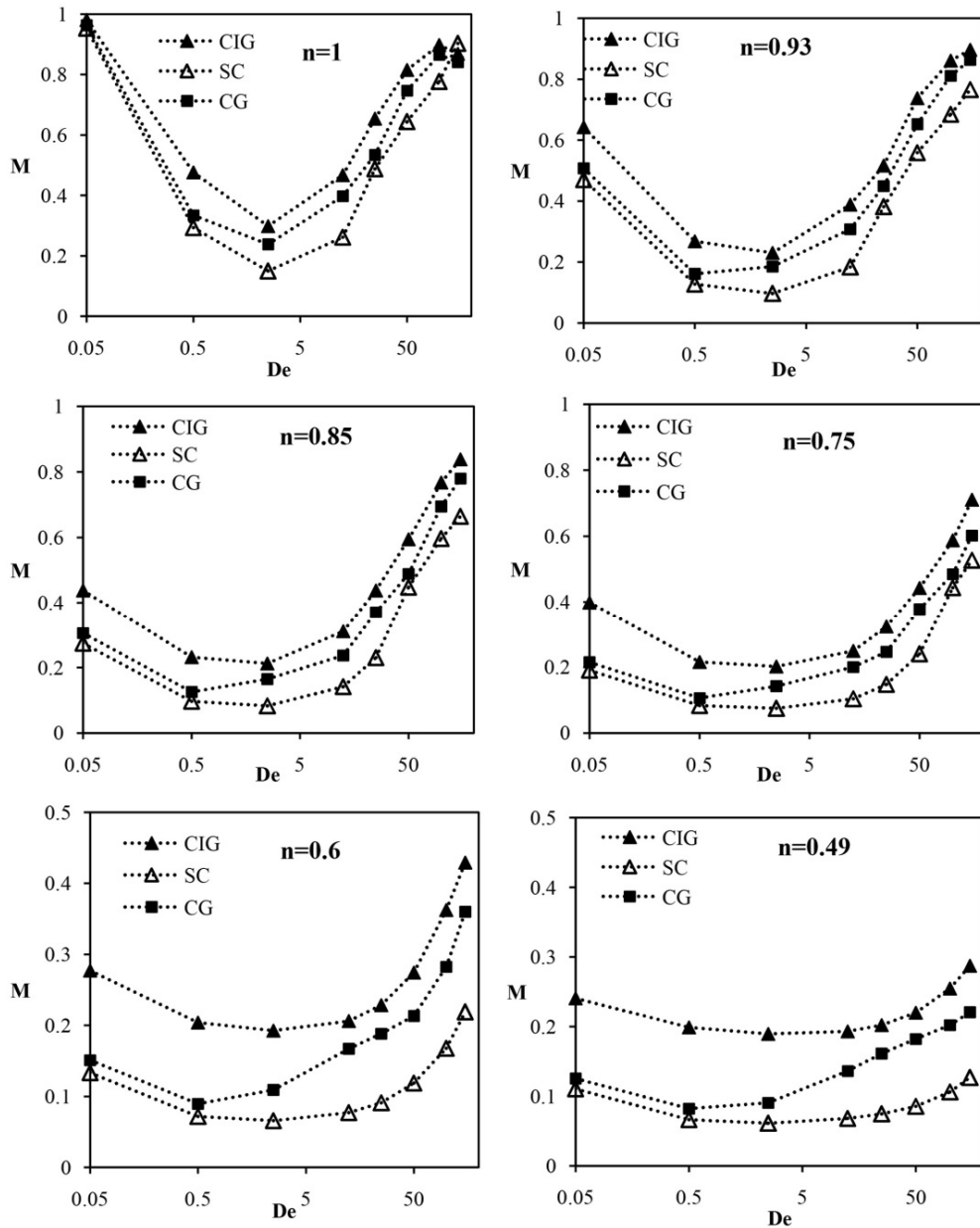


Fig. 14. Variations of the mixing index with the Dean number for various power-law indices and three micromixers, SC, CG and CIG ( $h=30 \mu\text{m}$ ,  $\theta=8.5^\circ$ ).

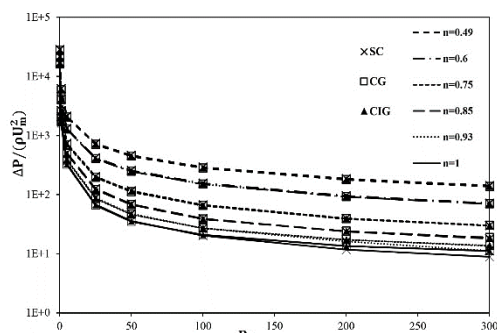


Fig. 15. Variations of the dimensionless pressure drop with the Reynolds number for various power-law indices and three micromixers, SC, CG and CIG ( $h=30 \mu\text{m}$ ,  $\theta=8.5^\circ$ ).

performance in curved micromixers such as adding baffles on the walls of mixing channel, splitting and recombining the flow in mixing channel, and etc. Although most of the methods improve the mixing quality, they cause a significant increase in pressure drop. But, in the present method while the degree of mixing increases, the non-dimensional pressure drop remains constant. This can be an important advantage of this method in comparison to the other methods.

In order to consider the combined effect of mixing index and pressure drop along the micromixers, a dimensionless parameter was defined as  $M/(\Delta P/\rho U_m^2)$ . The ratio of this parameter, for various grooved micromixers, to the SC-

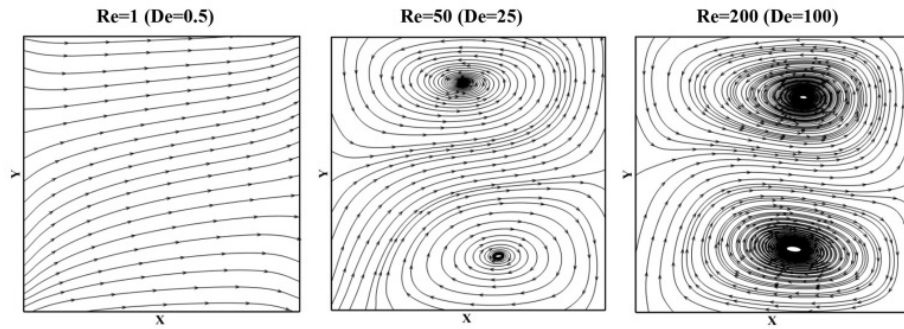


Fig. 16. The streamlines on Section-B of CIG-micromixer for  $n=0.85$  at various Reynolds (Dean) number,  $h=30 \mu\text{m}$ ,  $\theta=8.5^\circ$ .

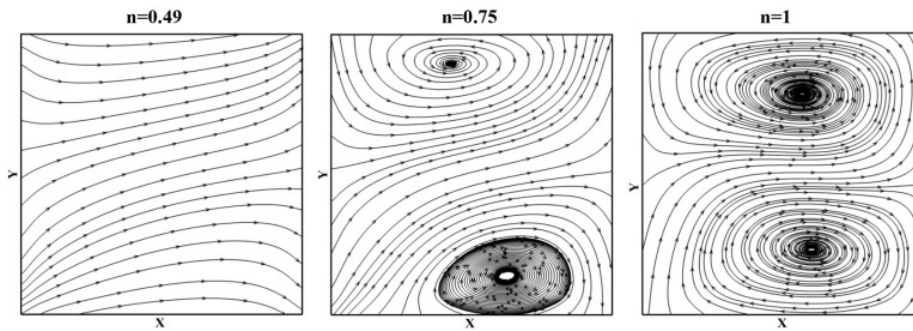


Fig. 17. The streamlines on Section-B of CIG-micromixer for various power-law indices,  $Re=50$  ( $De=25$ ),  $h=30 \mu\text{m}$ ,  $\theta=8.5^\circ$ .

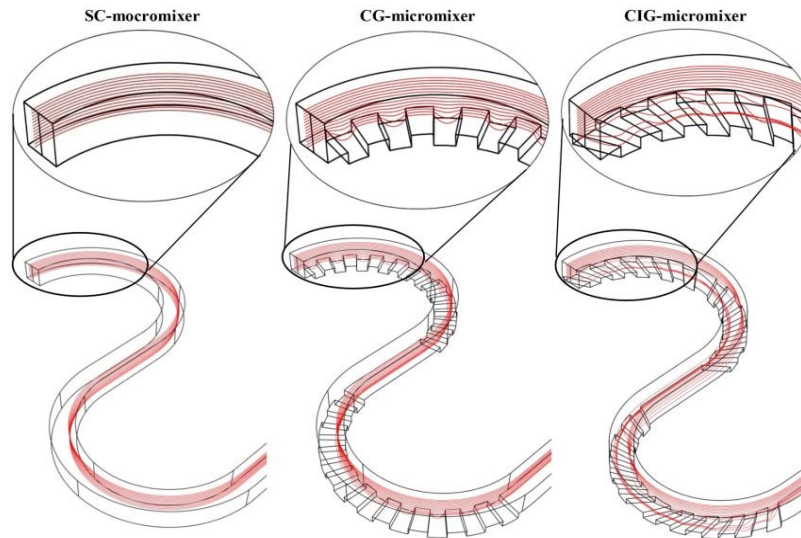


Fig. 18. Streamlines of velocity fields in different micromixers,  $n=0.85$ ,  $Re=1$  ( $De=0.5$ ),  $h=30 \mu\text{m}$ ,  $\theta=8.5^\circ$ .

Table 3 Ratio of  $M/(\Delta P/\rho U_m^2)$  for various grooved micromixers to the SC-micromixer

De	n=1			n=0.75			n=0.49		
	0.05	2.5	50	0.05	2.5	50	0.05	2.5	50
CG ( $h=30 \mu\text{m}$ , $\theta=8.5^\circ$ )	1.06	1.67	1.12	1.18	1.99	1.63	1.19	1.56	2.23
CG ( $h=30 \mu\text{m}$ , $\theta=6^\circ$ )	1.03	1.34	1.04	1.10	1.84	1.39	1.10	1.47	1.95
CG ( $h=30 \mu\text{m}$ , $\theta=3.5^\circ$ )	1.01	1.31	1.01	1.04	1.48	1.15	1.04	1.21	1.59
CG ( $h=15 \mu\text{m}$ , $\theta=8.5^\circ$ )	1.05	1.35	1.04	1.10	1.31	1.40	1.10	1.14	1.70
CG ( $h=15 \mu\text{m}$ , $\theta=6^\circ$ )	1.03	1.30	1.03	1.06	1.31	1.23	1.06	1.12	1.67
CG ( $h=15 \mu\text{m}$ , $\theta=3.5^\circ$ )	1.01	1.19	1.02	1.03	1.23	1.10	1.03	1.06	1.44
CIG	1.07	2.09	1.23	2.17	2.82	1.91	2.27	3.25	2.68

micromixer was calculated. A summary of these results is presented in Table 3. As can be seen, this ratio is greater than one for all cases. As well, CIG-micromixer has the highest value for all values of Reynolds number and power-law indices.

## 6. CONCLUSIONS

In this study, mixing of Newtonian and non-Newtonian fluids in a simple curved micromixer was investigated, numerically. Then the effect of grooves embedded on the bottom wall of micromixer and geometrical parameters such as depth and angle of grooves on mixing performance was examined. Moreover, the effect of angled grooves on mixing performance was examined. Water and CMC solutions with various mass fractions were selected as Newtonian and non-Newtonian fluids, respectively. For all studied cases, the results showed that the dimensionless pressure drops decreased rapidly by increasing Reynolds number and mixing index decreased by decreasing the power-law index. The groove depth and groove angle had no effect on mixing index at very low Reynolds numbers, but for non-Newtonian fluids at high Reynolds numbers, the mixing index increased by increasing the groove depth and groove angle. The inclined grooves caused the flow to become more chaotic, thus the mixing index of CIG-micromixer was better than the other micromixers, for all values of power-law indices. Also, in a given power law index, the grooves embedded on bottom wall of micromixer had no significant effect on dimensionless pressure drop.

## REFERENCES

- Afzal, A. and K. Y. Kim (2013). Mixing performance of passive micromixer with sinusoidal channel walls. *Journal of Chemical Engineering of Japan* 46(3), 230–238.
- Afzal, A. and K. Y. Kim (2014). Flow and mixing analysis of non-Newtonian fluids in straight and serpentine microchannels. *Chemical Engineering Science* 116, 263–274.
- Alam, A. and K. Y. Kim (2012). Analysis of mixing in a curved microchannel with rectangular grooves. *Chemical Engineering Journal* 181, 708–716.
- Ansari, M. A., K. Y. Kim, K. Anwar and S. M. Kim (2010). A novel passive micromixer based on unbalanced splits and collisions of fluid streams. *Journal of Micromechanics and Microengineering* 20, 055007–1–10.
- Cho, C. C., C. L. Chen and C. K. Chen (2012). Mixing of non-Newtonian fluids in wavy serpentine microchannel using electrokinetically driven flow. *Electrophoresis* 33(5), 743–750.
- Cook, K. J. and I. Hassan (2013). Experimental and numerical evaluation of a scaled-up micromixer with groove enhanced division elements. *Journal of Fluids Engineering* 135(1), 011201–1–14.
- Cook, K. J., Y. F. Fan and I. Hassan (2013). Mixing evaluation of a passive scaled-up serpentine micromixer with slanted grooves. *Journal of Fluids Engineering* 135(8), 081102–1–12.
- Das, T. and S. Chakraborty (2009). Biomicrofluidics: Recent trends and future challenges. *Sadhana* 34(4), 573–590.
- Delplace, F. and J. C. Leuliet (1995). Generalized Reynolds number for the flow of power law fluids in cylindrical ducts of arbitrary cross-section. *The Chemical Engineering Journal and the Biochemical Engineering Journal* 56(2), 33–37.
- Du, Y., Z. Zhang, C. Yim, M. Lin and X. Cao (2010). Evaluation of floor-grooved micromixers using concentration-channel length profiles. *Micromachines* 1, 19–33.
- Fellouah, H., C. Castelain, A. Ould-El-Moctar and H. Peerhossaini (2010). The Dean instability in power-law and Bingham fluids in a curved rectangular duct. *Journal of Non-Newtonian Fluid Mechanics* 165(3-4), 163–173.
- Hadigol, M., R. Nosrati, A. Nourbakhsh, M. Raisee (2011). Numerical study of electroosmotic micromixing of non-Newtonian fluids. *Journal of Non-Newtonian Fluid Mechanics* 166(17-18), 965–971.
- Jeong, G. S., S. Chung, C. B. Kim and S. H. Lee (2010). Applications of micromixing technology. *Analyst* 135(3), 460–473.
- Liu, S., A. N. Harymak and P. E. Wood (2006). Laminar mixing of shear thinning fluids in a SMX static mixer. *Chemical Engineering Science* 61(6), 1753–1759.
- Metzner, A. B. and J. C. Reed (1955). Flow of non-Newtonian fluids: correlation of the laminar, transition, and turbulent-flow regions. *American Institute of Chemical Engineers Journal* 1(4), 434–440.
- Nguyen, N. T. and Z. Wu (2005). Micromixers—a review. *Journal of Micromechanics and Microengineering* 15, 1–16.
- Pinho, F. T. and J. H. Whitelaw (1990). Flow of non-Newtonian fluids in pipe. *Journal of Non-Newtonian Fluid Mechanics* 34(2), 129–144.
- Rahmani, R. K., T. G. Keith and A. Ayasoufi (2004, July). Numerical simulation and mixing study of non-Newtonian fluids in an industrial helical static mixer. In *Proceedings of the ASME Heat Transfer/Fluids Engineering Summer Conference*, New York, USA.
- Scherr, T., C. Quitadamo, P. Tesvich, D. S. W. Park, T. Tiersch, D. Hayes, J. W. Choi, K. Nandakumar and W. T. Monroe (2012). A planar microfluidic mixer based on logarithmic spirals. *Journal of Micromechanics and Microengineering* 22(5), 055019–1–10.

- Srisamran, C. and S. Devahastin (2006). Numerical simulation of flow and mixing behavior of impinging streams of shear-thinning fluids. *Chemical Engineering Science* 61(15), 4884–4892.
- Tsai, R. T. and C. Y. Wu (2011). An efficient micromixer based on multi directional vortices due to baffles and channel curvature. *Biomicrofluidics* 5(1), 014103–1–13.
- Tsai, R. T. and C. Y. Wu (2012). Multidirectional vortices mixing in three-stream micromixers with two inlets. *Microsystem Technologies* 18(6), 779–786.
- Vanka, S. P., G. Luo and C. M. Winkler (2004). Numerical study of scalar mixing in curved channels at low Reynolds numbers. *American Institute of Chemical Engineers Journal* 50(10), 2359–2368.
- Wang, H., P. Iovenitti, E. Harvey and S. Masood (2003). Numerical investigation of mixing in microchannels with patterned grooves. *Journal of Micromechanics and Microengineering* 13(6), 801–808.
- Wanga, L. and K. C. Cheng (1996). Flow transitions and combined free and forced convective heat transfer in rotating curved channels: The case of positive rotation. *Physics of Fluids* 8(6), 1553–1573.
- Wu, C. Y. and R. T. Tsai (2013). Fluid mixing via multidirectional vortices in converging diverging meandering microchannels with semi-elliptical side walls. *Chemical Engineering Journal* 217, 320–328.
- Ziman, H. (1990). *A computer Prediction of Chemically Reacting Flows in Stirred Tanks*. Ph. D. thesis, University of London, UK.